Large-Area Sb_2Te_3 Nanowire Arrays

Chuangui Jin,[†,‡,§] Genqiang Zhang,[†,‡] Tian Qian,[†,‡] Xiaoguang Li,*[,†,‡] and Zhen Yao[||]

Hefei National Laboratory for Physical Science at Microscale, Department of Materials Science and Engineering, University of Science and Technology of China, Hefei 230026, China, International Center for Materials Physics, Academia Sinica, Shenyang 110015, China, College of Chemical Engineering and Environment, Anhui University of Technology, Maanshan 243002, China, and Department of Physics, University of Texas at Austin, Texas 78712

Received: August 29, 2004; In Final Form: November 2, 2004

High-density large-area nanowire arrays of thermoelectric material Sb_2Te_3 have been successfully prepared using electrochemical deposition into the channels of the porous anodic alumina membrane. The morphologies, structure, and composition of the as-prepared Sb_2Te_3 nanowires have been characterized using field-emission scanning electron microscopy, transmission electron microscopy, high-resolution transmission electron microscopy, X-ray diffraction, and X-ray photoelectron spectroscopy. Individual Sb_2Te_3 nanowires are single crystalline and continuous with uniform diameters (∼50 nm) throughout the entire length. The atomic ratio of Sb to Te is very close to the 2:3 stoichiometry.

Introduction

There is a growing interest in nanostructured thermoelectric (TE) materials because of the promise that the quantum confinement effect will increase the efficiencies of these materials as compared with their bulk counterparts.[1] This stimulates study in the preparation of nanowires of TE materials because nanowires are the most highly confined materials that still retain electrical connectivity. A single nanowire cannot transport enough current for TE applications. Therefore, the fabrication of high-density, large-area nanowire arrays is of particular importance. Many kinds of TE material nanowire arrays, such as Bi_2Te_3, $Bi_{1-x}Sb_x$, $Bi_{2-x}Sb_xTe_3$, and $Bi_2Te_{3-y}Se_y$,[2−5] have been prepared. Our previous work[6] has shown that Bi_2Te_3 nanowire arrays with high filling rate, aspect ratio, and large area can be directly deposited by electrochemical reduction of $HTeO_2^+$ and Bi^{3+} from an acidic aqueous solution using uniformly sized, parallel, and high aspect ratio porous anodic alumina membrane (PAAM) as templates.[7−10]

Antimony telluride belongs to layered semiconductors with tetradymite structure. This compound and its doped derivatives are considered to be the best candidates for near room-temperature TE applications.[11] Commonly, Sb_2Te_3 is obtained by chemical precipitation from an aqueous solution Sb^{3+} with H_2Te[12] or from sintering the elements.[13] Thin films are also obtained by means of sputtering,[14] metallorganic chemical vapor deposition (MOCVD),[15] flash evaporation,[16] and electrodeposition onto an indium tin oxide (ITO) substrate.[17] Because the Sb^{3+} is easy to hydrolyze and precipitate, it is difficult to obtain a relatively high concentration of Sb^{3+}, electrochemical deposition of compounds of Sb^{3+} is very difficult in aqueous solution, and the electrodeposition of the Sb_2Te_3 nanowires is quite challenging. To the best of our knowledge, the fabrication of the antimony telluride nanowire arrays has not been reported in the literature yet. In this paper, large-area, high filling rate, and highly ordered antimony telluride arrays have been successfully prepared in PAAM templates using a simple electrochemical deposition technique under suitable conditions at room temperature.

Experimental Procedures

The homemade PAAM templates were prepared using a two-step anodization process.[18,19] A layer of Au film was sputtered onto one side of the through-hole PAAM template to serve as the working electrode in a two-electrode electrochemical cell, and a graphite plate was used as the counter electrode. The antimony telluride nanowires were electrochemically deposited at a constant current density of 0.5 mA/cm^2 for 2 h in a glass cell at room temperature, which was strictly controlled by a potentiostat/galvanostat (HDV-7C); the volume of the electrobath was about 100 mL. The electrolyte solution consisted of 0.075 M $HTeO_2^+$ and 0.05 M SbO^+, and the pH of it is equal to 1. If the pH value of the electrolyte solution is too high, it will cause $HTeO_2^+$ and SbO^+ to hydrolyze and precipitate, and if it is too low, it will erode the PAAM template. The electrolyte solution is prepared as follows: to dissolve the $SbCl_3$ and avoid Sb^{3+} hydrolysis and precipitation, citric acid and potassium citrate were added to form an Sb−citric complex in one beaker by being heated, and the $HTeO_2^+$ came from the dissolved Te in 5 M HNO_3 by being heated in another beaker. Then, two beakers were mixed together, and distilled water and 5 M HNO_3 were added to reach the final volume and pH in the volumetric flask.

The templates gradually turn black during electrodeposition. When electrodeposition occurs on the surface of the templates, the potential suddenly increases because of larger area surface electrodeposition. After electrodeposition, the black antimony telluride nanowire arrays/PAAM template samples were obtained, rinsed with distilled water and absolute ethanol, and then dried in air at room temperature for further analysis.

The morphologies and structure of the Sb_2Te_3 nanowires were studied using X-ray diffraction (XRD, MXPAHF) with CuKα

* To whom correspondence should be addressed. Tel: +86-551-3603408; fax: +86-551-3603408; e-mail: lixg@ustc.edu.cn
[†] University of Science and Technology of China.
[‡] International Center for Materials Physics.
[§] Anhui University of Technology.
[||] University of Texas at Austin.

10.1021/jp046100z CCC: $30.25
Published on Web 01/08/2005

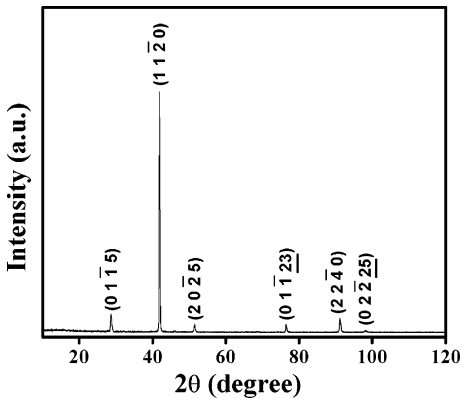

Figure 1. XRD pattern of Sb_2Te_3 nanowires.

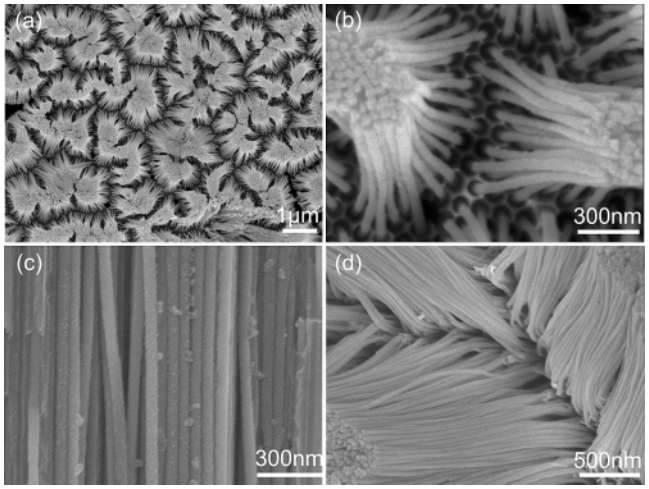

Figure 2. SEM images of Sb_2Te_3 nanowire array after the template is partially etched. Panels a and b are top views after 5 min of etching. Panels c and d are side and top views after 10 min of etching, respectively.

radiation ($\lambda = 1.5406$ Å) in the range of $10° \leq 2\theta \leq 120°$; field-emission scanning electron microscopy (FE-SEM, JEOL, JSM-6700F); transmission electron microscopy (TEM, Hitachi-800); and high-resolution transmission electron microscopy (HRTEM, JEOL-2010). The chemical composition of the nanowires was determined by X-ray photoelectron spectroscopy (XPS, VGESCALAB MK-II).

Results and Discussion

The XRD pattern of the as-prepared sample is shown in Figure 1. All the peaks can be indexed to the hexagonal Sb_2Te_3 structure with cell constants $a = 0.426$ nm and $c = 3.05$ nm (JCPDS No. 15-874). The intensity for $(11\bar{2}0)$ is much higher than those for the other peaks, indicating that the Sb_2Te_3 nanowires have preferential orientation along the $[11\bar{2}0]$ direction, which will be further confirmed by HRTEM results.

Figure 2a−d shows the FE-SEM morphologies of the Sb_2Te_3 nanowires in the PAAM template. Figure 2a,b is different magnification FE-SEM micrographs of the Sb_2Te_3 nanowires after the PAAM template has been etched in 1 M NaOH for 5 min. From Figure 2a, a high nanopore filling efficiency (100%) and high homogeneity over a large area can be observed. Figure 2b,c is a surface and a cross-sectional FE-SEM image of the nanowire arrays after the template has been etched for 5 and 10 min, respectively. They clearly display that the Sb_2Te_3 nanowire arrays are ordered, continuous, dense, and uniform in diameter and length, that the cylindrical nanowires grow from the perfect hexagonal cells of the template, and that the surface of the nanowires is smooth. The beautiful flower formations, as shown in Figure 2a,b, probably result from the action of capillary forces that gather the vertical nanofibers into bundles, but supercritical drying can be used to avoid the detrimental action of capillary forces. Figure 2d is a typical FE-SEM surface image of the sample with an eroding time of 10 min. It is clear that the exposed length of the Sb_2Te_3 nanowires increases with an increase in the eroding time.

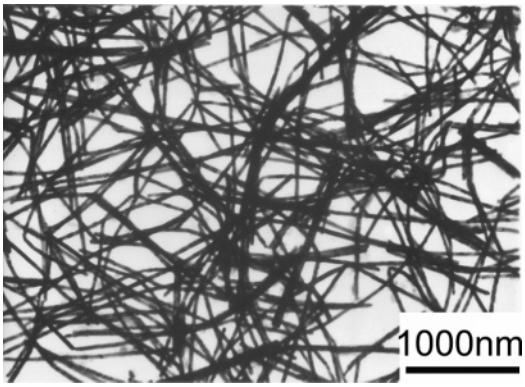

Figure 3. TEM image of Sb_2Te_3 nanowires.

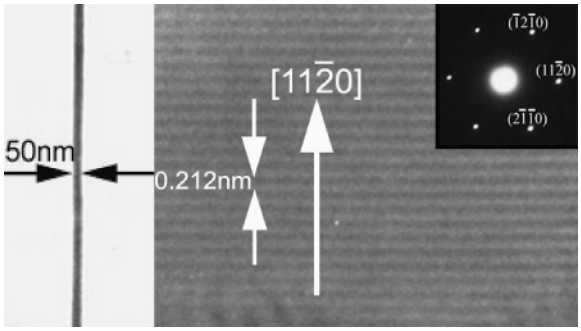

Figure 4. TEM and HRTEM images of the same single Sb_2Te_3 nanowire; the inset is the corresponding ED pattern.

A representative TEM image of the Sb_2Te_3 nanowires is shown in Figure 3. It is clear that the diameters are uniform and the length of the nanowires is up to tens of micrometers. Because the electrodeposition follows a bottom-up mechanism, namely, the Sb_2Te_3 nucleates at the bottom of the pores and grows along the pores to the top, the length of the nanowires is the same as the thickness of the template used.

HRTEM images provide further insight into the structures of the Sb_2Te_3 nanowires. Figure 4 shows a typical HRTEM image of a single Sb_2Te_3 nanowire and the corresponding ED pattern. The diameter of the nanowire is highly uniform and appears rather homogeneous. The nanowires are free of observable defects, and ED patterns are bright spots, suggesting single crystallinity of the Sb_2Te_3 nanowires. The diffraction spots of the $(11\bar{2}0)$, $(\bar{1}2\bar{1}0)$, and $(2\bar{1}\bar{1}0)$ correspond to lattice planes of the single-crystal hexagonal packed structure of Sb_2Te_3. Calculation results indicate that the incident beam is parrllel to the [0001] direction. The lattice-resolved image of the representative nanowire further reveals that the nanowires are structurally uniform and single crystalline, with an interplanar spacing of 0.212 nm corresponding to the $\{11\bar{2}0\}$ distance of hexagonal Sb_2Te_3.

The composition of Sb_2Te_3 is determined by XPS. The XPS data were collected in the constant analyzer energy mode at 20 eV. MgKα ($h\nu = 1253.6$ eV) radiation was employed as the excitation source with an anode voltage of 12 kV and an

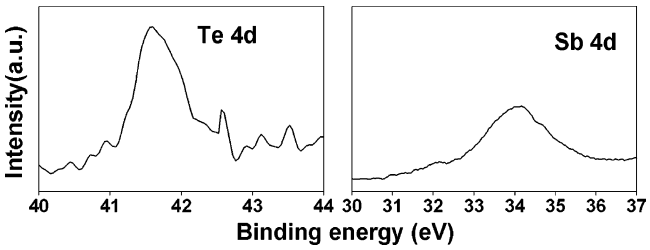

Figure 5. XPS of the Sb_2Te_3 nanowires.

emission current of 20 mA. The binding energies of Te_{4d} and Sb_{4d} are 41.52 and 33.91 eV, respectively, as seen in Figure 5, which are in good agreement with those of the Sb_2Te_3 bulk material (41.4 and 33.78 eV, respectively).[20] The quantification of the peaks gives a ratio of Sb/Te = 2.1:2.9, and no other peaks were observed, demonstrating that stoichiometric Sb_2Te_3 nanowires were formed.

The electrodeposition process of the Sb_2Te_3 nanowires mainly involves the following four steps:

(i) $HTeO_2^+$ and SbO^+ diffuse to the Au electrode surface and are adsorbed on the surface by the electric field force.

(ii) The adsorbed $HTeO_2^+$ and SbO^+ get electrons to produce elemental Te and Sb by the reactions

$$HTeO_2^+ + 3H^+ + 4e = Te(s) + 2H_2O \quad (1)$$

$$SbO^+ + 2H^+ + 3e = Sb(s) + 3H_2O \quad (2)$$

(iii) The reduced Te and Sb atoms react with each other to form Sb_2Te_3. Thus, the overall reaction can be expressed as

$$3HTeO_2^+ + 2SbO^+ + 13H^+ + 18e = Sb_2Te_3(s) + 8H_2O \quad (3)$$

(iiii) Sb_2Te_3 nucleates and grows in the nanochannels of the template.

Step i is a rate-determining step, which is controlled by the current density. Step ii seems to proceed rapidly. Steps i−iii can affect the composition of the nanowires. Step iiii affects the crystallinity of the nanowires.[21]

To synthesize large-area, high-filling, and single-crystal Sb_2Te_3 nanowire arrays, several factors seem to play an important role. First, the PAAM templates pretreatment of the electrodeposition is necessary, such as sonication cleaning and vacuum driving out air trapped inside the nanochannels of the templates and perfusing electrolyte solution into the nanochannels of the templates. If there are impurities in the nanochannels or the surface of the PAAM templates, Sb_2Te_3 will preferentially nucleate and grow at the site of the impurities, causing inhomogeneous nucleation and growth and making it difficult to prepare high filling and dense nanowire arrays. If there is air in the nanochannels, it will hinder the ions to diffuse the surface of the Au electrode, and nanowires may be deposited on the surface of the PAAM templates, not in the nanochannels of the templates. Therefore, it is also impossible to fabricate high-filling and continuous nanowire arrays. Second, if the rate of reaction, nucleation, and growth is faster than that of ion diffusion, it will cause a lack of ions near the Au electrode or in the nanochannels of the PAAM templates, resulting in concentration gradient. To avoid the rapid nucleation, growth, and concentration gradient, we tried to minimize the rate of the nucleation and growth by reducing the concentrations of $HTeO_2^+$ and SbO^+ in our experiment because the slower growth rate can increase the crystallinity of the nanowires, filling-rate, and compositional homogeneity.[5] Other factors, such as temperature,[22] structural integrity of the template,[2] pH value, current density, or deposition potential, are also important. Only at optimal conditions can large-area and stoichiometric Sb_2Te_3 nanowire arrays with a high-filling ratio be fabricated.

Conclusion

In summary, we have used a simple direct current electrodeposition process to fabricate large-area Sb_2Te_3 nanowire arrays using PAAM templates. FE-SEM, TEM, and HRTEM investigation results show that the Sb_2Te_3 nanowire arrays are dense, parallel, and large-area, with 100% of the pores of the PAAM templates filled. We believe that this simple approach can be generalized to controllably produce a variety of nanowires of interesting nanotechnological applications.

Acknowledgment. This work was supported by the National Natural Science Foundation of China.

References and Notes

(1) Harman, T. C.; Taylor, P. J.; Walsh, M. P.; Laforge, B. E. *Science* **2002**, *297*, 2229.
(2) Prieto, A. L.; Sander, M. S.; González, M. M.; Gronsky, R.; Sands, T.; Stacy, A. M. *J. Am. Chem. Soc.* **2001**, *123*, 7160.
(3) Lin, Y. M.; Rabin, O.; Cronin, S. B.; Ying, J. K.; Dresselhaus, M. S. *Appl. Phys. Lett.* **2002**, *81*, 2403.
(4) González, M. M.; Prieto, A. L.; Gronsky, R.; Sands, T.; Stacy, A. M. *Adv. Mater.* **2003**, *15*, 1003.
(5) González, M. M.; Snyder, G. F.; Prieto, A. L.; Gronsky, R.; Sands, T.; Stacy, A. M. *Nano Lett.* **2003**, *7*, 973.
(6) Jin, C. G.; Xiang, X. Q.; Jia, C.; Liu, W. F.; Cai, W. L.; Yao, L. Z.; Li, X. G. *J. Phys. Chem. B* **2004,** *108*, 1844.
(7) Thompson, G. E.; Furneaux, R. C.; Wood, G. C.; Richardson, J. A.; Goode, J. S. *Nature* **1978**, *272*, 433.
(8) Li, A. P.; Müller, F.; Birner, A.; Nielsh, K.; Gösele, U. *J. Appl. Phys.* **1998**, *84*, 6023.
(9) Li, F.; Zhang, L.; Metzger, R. M. *Chem. Mater.* **1998**, *10*, 2470.
(10) Shingubara, S.; Okino, O.; Sayama, Y.; Sakaue, H.; Takahagi, T. *Jpn. J. Appl. Phys.* **1997**, *36*, 7791.
(11) Venkatasubramanian, R.; Siivola, E.; Colpitts, T.; Quinn, B. O. *Nature* **2001**, *413*, 597.
(12) Bruckl, A. *Monatsh. Chem.* **1925**, *45*, 483.
(13) Oppenheimer, A. *J. Prakt. Chem.* **1857**, *71*, 277.
(14) Romeo, N.; Bosio, A.; Tedeschi, R.; Romeo, A.; Canevari, V. *Sol. Energy Mater. Sol. Cells.* **1999**, *58*, 209.
(15) Giani, A.; Boulouz, A.; Delannoy, F. P.; Foucaran, A.; Boyer, A.; Aboulfarah, B.; Mzerd, A. *J. Mater. Sci. Lett.* **1999**, *18*, 541.
(16) Patel, T. C.; Patel, P. G. *Mater. Lett.* **1984**, *3*, 2.
(17) Leimkühler, G.; Kerkamm, I.; Reineke-Koch, R. *J. Electrochem. Soc.* **2002**, *149*, C474.
(18) Masuda, H.; Fukuda, K. *Science* **1995**, *268*, 1466.
(19) Masuda, H.; Hasegwa, F.; Ono, S. *J. Electrochem. Soc.* **1997**, *144*, L127.
(20) Wagner, C. D.; Riggs, W. M.; Davis, L. E.; Moulder, J. F.; Muilenberg, G. E. *Handbook of X-ray Photoelectron Spectroscopy*; Perkin-Elmer Corporation: Eden Prairie, MN, 1979.
(21) Takahashi, M.; Oda, Y.; Ogino, T.; Furuta, S. *J. Electrochem. Soc.* **1993**, *9*, 2550.
(22) Mochizuki, K.; Jin, Y. X.; Chu, T. L. *J. Cryst. Growth* **1984**, *67*, 420.